Propagation and interference of thermal waves in turbulent thermal convection

P. Urban [1], T. Králík,[1] V. Musilová,[1] D. Schmoranzer [2], and L. Skrbek [2]

[1]*The Czech Academy of Sciences, Institute of Scientific Instruments,*
Královopolská 147, 612 00 Brno, Czech Republic

[2]*Faculty of Mathematics and Physics, Charles University, Ke Karlovu 3, 121 16, Prague, Czech Republic*

We report investigation of thermal waves in harmonically modulated turbulent thermal convection in a Rayleigh-Bénard cell. We probe the thermal waves in the working fluid—cryogenic helium gas—by temperature sensors placed in the cell and embedded in the plates. We observe propagation and interference of two coherent thermal waves and describe their behavior in terms of models that explain the weak attenuation and apparent superposition of thermal waves in the bulk, accounting for the temperature profile of convective turbulent flow via a spatially dependent effective thermal diffusivity.

I. INTRODUCTION

A. Thermal waves

Waves can be generally understood as organized propagating imbalances [1]. Thermal or heat waves [2], temperature oscillations resulting from periodic heating/cooling of heat-conducting materials, can be described as solutions of parabolic heat diffusion equation in the presence of a harmonically varying heat source. A simple way to introduce thermal waves propagating in solids or in quiescent fluids of density ρ, and thermal capacity c is to consider an isotropic homogeneous semi-infinite cylinder of unit cross section with its end surface subject to uniformly distributed harmonically modulated heat flux. The temperature distribution $T(z, t)$ within such a rod can be obtained by solving the one-dimensional parabolic heat diffusion equation $\partial^2/\partial z^2[T(z, t)] = (1/\kappa)\partial/\partial t[T(z, t)]$, subject to the boundary conditions $\lambda\,\partial T/\partial z|_{z=0} = -\dot{q}[1 + \cos(\omega_m t)]$, and $T(z, t)|_{z\to\infty} = const.$, where $\omega_m = 2\pi f_m$ is the angular frequency of modulation, κ stands for the thermal diffusivity, related to the thermal conductivity $\lambda = \kappa c\rho$. The heating consists of two contributions, which produce: (i) a steady temperature profile (as per Fourier law) and (ii) a propagating thermal wave of the form

$$T(z, t) = \frac{\dot{q}}{\rho c\sqrt{\kappa\omega_m}}\exp\left(-\frac{z}{\delta}\right)\cos\left(\omega_m t - \frac{z}{\delta} - \frac{\pi}{4}\right), \tag{1}$$

where $\delta = \sqrt{2\kappa/\omega_m}$ denotes the thermal diffusion length. The amplitude of this thermal wave is decreasing exponentially whereas the phase delay increases linearly with the propagation distance. There is a phase lag of $\pi/4$ between the applied heat and the temperature $T(0, t)$. Thermal waves with the phase velocity $u_p = \omega_m\delta$ are highly dispersive and heavily damped with the decay constant equal to the thermal diffusion length. This simple description of thermal waves is valid also for quiescent viscous fluids. For finite-size systems, the wave profile would be modified accordingly, as determined by the boundary conditions. The applications of thermal waves go back to 1863, when Ångström [3] used them to determine thermal diffusivity of materials.

We note that the parabolic heat diffusion equation has the following unphysical property: as first noted by Cattaneo [4], a sudden change in temperature in one spot will be felt instantly everywhere,

063501-1
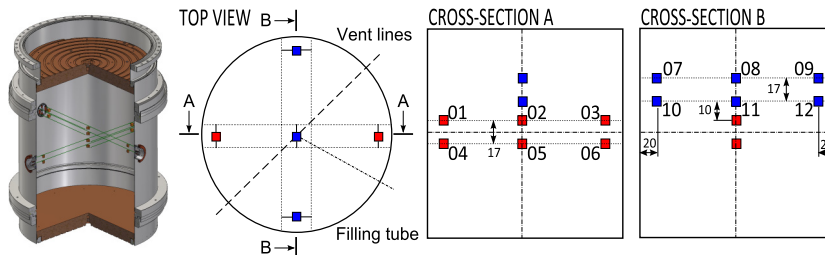
FIG. 1. Left: Schematic of the aspect ratio one RBC cell 30 cm in diameter [16]. Both the top and bottom plates are made of 28-mm thick annealed copper of very high thermal conductivity; their temperatures $T_t(t)$ and $T_b(t)$ are read by the embedded precisely calibrated Ge sensors [17]. The instantaneous temperature of the working fluid, cryogenic helium gas, is monitored by tiny temperature sensors [18–20] home-calibrated within 1-mK accuracy against the primary Ge sensors, installed in the cell interior using 0.1-mm constantan wires as shown (distances in millimeters).

giving rise to infinite speed of heat propagation. To solve this issue, a hyperbolic heat diffusion equation, which includes an inertial term describing a delay between the temperature gradient and the heat flow has been proposed [2,5].

B. Thermal waves in turbulent fluids

Interestingly, thermal waves are readily observed in superfluids, such as helium cooled below $T_\lambda \approx 2.17$ K where within the two-fluid model, they result from a wave-type equation and take the form of a so-called second sound [6]. This temperature/entropy wave complements the usual pressure/density wave ("first sound" in the context of superfluids) and propagates with very weak attenuation, allowing for practical construction of second sound resonators, which represent a very useful tool to investigate quantum turbulence in superfluid helium [6,7]. It follows naturally to compare the effects of turbulent flow on classical thermal waves in the Rayleigh-Bénard convection (RBC) and on waves of second sound in superfluids or with recently observed second sound in the rapidly varying temperature field in Ge [8].

As for classical viscous flows, the behavior of thermal waves becomes more complex, due to the laminar or turbulent advection and diffusion of heat. Here, we are interested in properties and interference of thermal waves in highly turbulent RBC [9,10] where they can be coherently generated by a temperature modulation of either the top or bottom plate [11] of the RBC cell, see Fig. 1.

RBC is sensitive to temperature modulation of the plates, e.g., a slight modulation results in a shift of the critical Rayleigh number (Ra) for the the onset of convection [12,13]. As for turbulent RBC flow, early numerical studies [14,15] as well as the recent numerical two-dimensional study in the range of $10^7 \leqslant \mathrm{Ra} \leqslant 10^9$ (backed up by a three-dimensional simulations for Ra $= 10^8$) by Yang *et al.* [21] suggest that harmonic temperature modulation of plates leads to heat transfer efficiency enhancement. Using cryogenic helium gas of the Prandtl number (Pr) Pr ≈ 1 as a working fluid, our group recently confirmed such an enhancement experimentally for $10^8 \leqslant \mathrm{Ra} \leqslant 2 \times 10^{12}$ [11].

Thermal waves in turbulent RBC have been detected using a small Ge temperature sensor in the middle of a cryogenic RBC cell by Niemela and Sreenivasan [22]. They measured the modulation depth of the signal, which followed the modulated temperature $T_B(t) = A_{T0} \cos(\omega_m t)$ of the bottom plate. For moderate Ra $\approx 10^9$, the modulation depth $A_T(z,t)$ of the vertically propagating thermal wave agreed with the form

$$\frac{A_T(z,t)}{A_{T0}} = e^{-z/\delta_s} \cos\left(\omega_m t - \frac{z}{\delta_s}\right), \quad \delta_s = \sqrt{\frac{2\kappa_{\mathrm{eff}}}{\omega_m}}, \tag{2}$$

where δ_s denotes the Stokes layer thickness (thermal penetration depth) based on an enhanced effective thermal diffusivity $\kappa_{\text{eff}} = \text{Nu}\,\kappa$, where Nu represents the Nusselt number. However, the authors note that same approach failed to describe data taken at higher Ra $\approx 10^{13}$.

Let us point out here the most important difference between classical thermal waves and second sound in superfluids. Although second sound propagating in superfluids is heavily attenuated in the presence of quantum turbulence compared to the quiescent state [6], the attenuation of thermal waves propagating in classical fluids becomes significantly weaker when turbulence is introduced due to the enhanced thermal diffusivity, see Eq. (2). This seems to suggest that the high attenuation of thermal waves in quiescent classical fluids stems solely from the lack of convective heat transfer at low Ra, which, however, exists in superfluids in the form of thermal counterflow even for infinitesimally small temperature gradients and is, in fact, hindered by the onset of quantum turbulence. In consequence, it may prove interesting to investigate and test the following hypothesis: Once motion (inertia) of a working medium becomes associated with heat transfer, the observed attenuation of any thermal waves in the given system will be significantly suppressed. However, such investigation is beyond the scope of this paper, where no inertial effects are considered. Recently, a nonzero heat flux was reported for thermal waves [23] due to nonlinear effects associated with temperature-dependent thermal diffusivity. In our paper, similar effects could be observable as well, but not dominant, as thermal diffusivity of helium changes only by $\simeq 5\%$ in the experimental temperature range. Neglecting these nonlinearities, we use the traditional parabolic heat equation with a temperature-independent thermal diffusivity.

Our group recently extended measurements of propagating thermal waves in turbulent RBC, covering wide ranges of Ra, modulation frequencies f_m, and relative depth of temperature modulation of either plate, using several temperature sensors placed in the bulk of the RBC flow [11]. We have introduced a nondimensional scaling frequency $f_s = 1/(\pi\xi)\hat{f}\,\text{Ra}^{1/6}\text{Pr}^{1/2}$, where $\xi(\text{Ra})$ is a numerical factor ≈ 0.06, weakly decreasing with Ra and the nondimensional frequency $\hat{f} = f_m \tau_{ff}$ is scaled by the free fall time, $\tau_{ff} = (\text{Ra}\,\text{Pr})^{-1/2}L^2/\kappa$. We have shown that the attenuated amplitudes and phase shifts measured by sensors in the bulk at various Ra's, f_m and A_T, collapse on a single frequency dependence when plotted versus f_s.

In this paper we focus, besides the detailed description of propagation of thermal waves, on their constructive and destructive interferences.

II. EXPERIMENTAL RESULTS AND DISCUSSION

The obtained by us data confirm that Eq. (2) cannot accurately describe all observed details. First, the measured phase shift displayed a tendency to saturate near $\pi/2$ for $f_s > 1$ and, second, the differences between individual sensor readings in the bulk did not, within the experimental resolution, depend on their position [11], in contrast to Eq. (2). This is illustrated in the left panel of Fig. 2. That the turbulent bulk of the RBC flow is at all times nearly isothermal and near equilibrium (in a statistical sense, by virtue of separation of timescales), is independently confirmed by recording the pressure in the RBC cell (see the right axis of the left panel). When converted to temperature using the XHEPAK software [24] under the assumption of constant density in the entire RBC cell, it quantitatively agrees with the directly measured temperatures by the sensors in the bulk, collapsing onto a single trace. The middle and right panels in Fig. 2 show that the same outcome is observed when modulation is applied to either of the bounding plates. All experimental data shown for modulated RBC flow were taken under the following conditions of the corresponding statistically steady RBC flow: Ra $= 7 \times 10^{10}$, Nu $= 232$, and Pr $= 0.74$. Changing Ra by two orders of magnitude up or down does not appreciably affect the results.

In order to account for all the observed facts, we develop two physically motivated models (described in detail in the Appendix) and test them against propagation of a plane thermal wave and for interference of two thermal waves generated coherently by both plates of the RBC cell. Specifically, Model 1 takes into account the vertical structure of the high Ra turbulent RBC flow, namely, the existence of thermal and kinetic boundary layers (BLs), which for cryogenic He gas
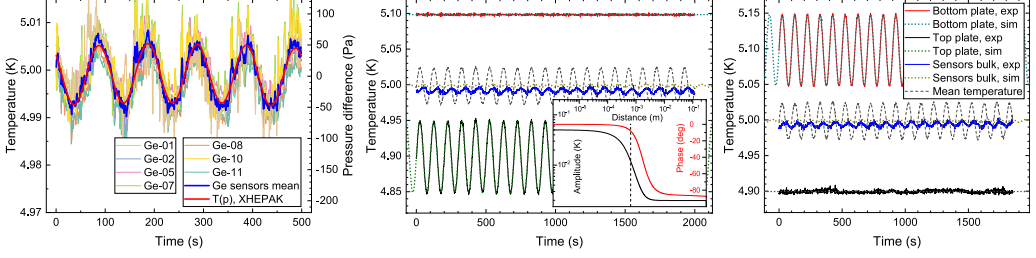
FIG. 2. Left: Temperature record of 7-Ge sensors in the bulk as indicated, together with their mean (blue) and the pressure trace (red) converted to temperature using the XHEPAK software [24] under the assumption of constant density $\rho_{He} = 3.607$ kg/m^3. The right axis corresponds to the original pressure trace taken as the difference from the equilibrium value, $p - p_0$, where $p_0 = 35\,260$ Pa. Readings of the 7 sensors in the bulk are, within the experimental resolution, identical. Middle and right: Readings of the two-plate thermometers and the (mean) bulk temperature plotted together with results of numerical simulations. The temperature wave in the bulk appears identical, irrespectively, of whether the top (middle panel) or bottom (right panel) plate temperature is modulated. The dotted lines represent calculated responses according to the theoretical Model 1. The offset between calculated and measured bulk values is caused by boundary layer asymmetry as explained in the text. The gray dashed line indicates the mean temperature $T_m(t) = [T_t(t) + T_b(t)]/2$. The inset in the middle panel shows the calculated variations of the thermal wave amplitude and phase with distance from the top plate. The dashed vertical line marks the boundary layer thickness ℓ_{BL}.

with Pr ≈ 1 are of similar thicknesses: $\ell_{BL} \simeq L/(2\,\mathrm{Nu})$. In accord with the dimensional reasoning of Priestley [25] and marginal stability arguments of Malkus [26], the high-Ra turbulent convective flow consists of (almost) isothermal bulk and two laminar BLs adjacent to plates, over which most of the temperature difference drops. With increasing Ra, ℓ_{BL} decreases and the temperature profile near the plates becomes steeper. In the statistically steady state of the turbulent RBC flow, the vertical temperature profile establishes, of the form closely following the analytical solution for Pr ≈ 1 by Shishkina *et al.* [27],

$$\theta = \frac{\sqrt{3}}{4\pi} \ln \frac{(1 + a\xi)^3}{1 + (a\xi)^3} + \frac{3}{2\pi} \arctan \left(\frac{4\pi}{9}\xi - \frac{1}{\sqrt{3}} \right) + \frac{1}{4}, \tag{3}$$

where $a = 2\pi/3\sqrt{3} \approx 1.2$ and a local similarity variable $\xi = z/\delta(x)$ where $\delta(x)$ stands for the local BL thickness, which we approximate as $\delta(x) \approx \ell_{BL} \simeq L/(2\,\mathrm{Nu})$ over the entire surface of the plates.

The vertical temperature gradient can be expressed via an effective heat conductivity $\lambda_{\mathrm{eff}}(z) = \kappa_{\mathrm{eff}}(z)c_p\rho$, where $\kappa_{\mathrm{eff}}(z)$ is the effective local thermal diffusivity, c_p is the thermal capacity at constant pressure, and ρ denotes the density of the working fluid. Experimental observations just described suggest that $\kappa_{\mathrm{eff}}(z)/\kappa$ (i.e., the local Nusselt number) in the bulk must be very large in accord with simulations of high-Ra RBC with periodic boundary conditions (i.e., effectively excluding BLs) [28]. This led to the suggestion of a "superconducting core" [22]. We then solve numerically the parabolic heat equation for a nonhomogeneous medium $\partial T/\partial t = \partial/\partial z[\kappa_{\mathrm{eff}}(z)\,\partial T/\partial z]$ for $T(z, t)$ in Fourier space, subject to the experimentally imposed boundary conditions. Details are given in the Appendix.

The middle and right panels in Fig. 2 show that Model 1 describes the experimental facts quantitatively: The amplitude of the propagating thermal wave decreases steeply within the BL and its vicinity, whereas in the turbulent bulk of the RBC flow its amplitude appears almost constant, in accord with the experimental observation, although the bulk wave amplitude is underestimated, see the Appendix. The inset in the middle panel shows that the changes in amplitude and phase of the propagating thermal wave occur almost entirely within the distance of a few ℓ_{BL}'s, which is marked by the vertical line.
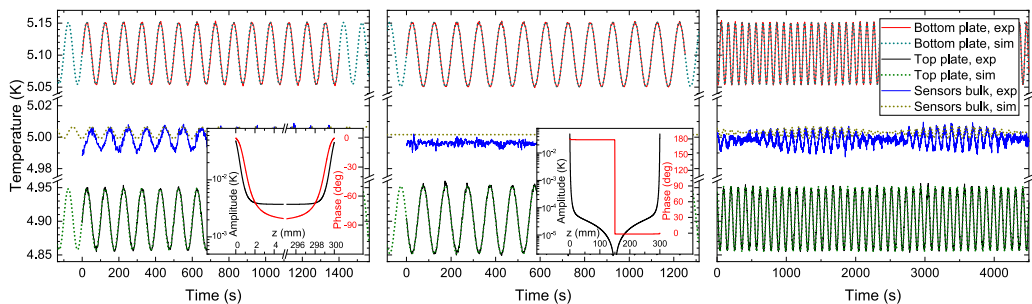
FIG. 3. Constructive (left panel) and destructive (middle panel) interference of thermal waves propagating coherently from the top and bottom plates obtained by modulating the plate temperatures in phase, or out of phase, respectively. The right panel illustrates interference in a form of beatings of thermal waves propagating from the top plate ($f_{mt} = 0.01$ Hz) and bottom plate ($f_{mb} = 0.0095$ Hz). Solid lines represent records of thermometers embedded in plates and the mean of sensors placed in the bulk (same as in Fig. 2), whereas dotted lines show values calculated using Model 1. The offset between the measured and calculated data is again due to BLs asymmetry. The insets show the calculated thermal wave amplitudes and phases for constructive and destructive interference.

We note that this model tends to underestimate the temperature wave amplitudes in the bulk. This is caused by the fact that κ_{eff} is determined from the steady-state BL only, i.e., no modulation of the BL properties is taken into account. A full-fledged description of the complex phenomena occurring in BLs under temperature modulation, such as enhancement of heat transfer efficiency and effects related to the ejection of thermal plumes is beyond the scope of this simple one-dimensional model.

There is an offset between the calculated and the measured bulk values, which exceeds the relative thermometer calibration uncertainties. It is caused by BL asymmetry [29]. Indeed in our previous work [30], we have measured and discussed "parameter x" defined as the ratio of the temperature drop over the top BL to that over the bottom BL—see it plotted versus Ra in Fig. 8 of Ref. [30]. For our RBC cell and experimental conditions related to the displayed data $x \approx 0.9$, which for the temperature difference between the plates $\Delta T = 200$ mK leads to the offset of ≈ 5 mK between the directly measured and the calculated temperature of the bulk, precisely as observed (Model 1 does not take this asymmetry into account).

Our thermally fast [31] experimental apparatus [11,16] allows to study interference of thermal waves, coherently generated by both plates. Figure 3 illustrates both constructive (left) and destructive (middle) interference of thermal waves generated simultaneously at both plates, by modulating their temperatures: the same amplitude of modulation applied in phase and out of phase. In the former case, the measured signal in the bulk is twice that as in Fig. 2; in the latter case of destructive interference the measured signal is vanishingly small.

Interference of thermal waves is even more clearly documented in the right panel of Fig. 3, which shows the directly measured time records of temperatures of plates as well as the mean of seven signals measured in various places in the turbulent bulk of the RBC flow. The same amplitude of temperature modulation is applied to both plates but at slightly different frequencies as indicated, leading to distinctly resolved beating patterns. The dotted lines are again solutions of Model 1 with boundary conditions matching the experiment. The insets show that, whereas in the case of constructive interference the calculated thermal wave amplitudes and phases change within the distance of few ℓ_{BL}'s and stay finite in the cell interior, for the case of destructive interference both the amplitude and the phase approach zero in the middle of the RBC cell.

We emphasize that, at low f_m, used in these experiments, the temperature of almost entire turbulent bulk oscillates synchronously as confirmed both directly by identical temperature records of sensors placed in various places and indirectly by converting the pressure record into temperature (see Fig. 2). For very high Ra (i.e., very thin BLs), our Model 1 can be simplified in the following

way: Both the top and the bottom plates as well as the bulk of the turbulent RBC flow are assumed to be ideal heat conductors; with the nearly superconducting [22] bulk core surrounded by thermal BLs of thickness $\ell_{BL} \simeq L/(2\,\mathrm{Nu}) \ll L$, negligibly small thermal capacity, and finite thermal conductance. Together with boundary conditions matching those experimentally applied as described above, this represents our Model 2. For details on this simple, analytically soluble model we direct the reader to the Appendix. For example, in the simplest case of constant bottom plate temperature with the top plate temperature harmonically modulated, Model 2 predicts that for $f_m \to 0$ the phase-shift $\phi \to 0$, for small f_m, it approximately linearly increases and, in the high-frequency limit, the phase saturates at $\pi/2$, and the temperature modulation in the bulk $A_c \to 0$, in qualitative agreement with our experimental observations. Although Model 1 provides a more detailed description of the BL and a more accurate estimate of the thermal wave amplitude in the bulk, Model 2 correctly predicts the phase saturation as observed [11]. Future work, both experimental and numerical, promises to reveal detailed properties of both steady and modulated thermal BLs using thermal waves as a probe.

III. CONCLUSIONS

We have utilized a thermally fast RBC cell to study generation, propagation, and interference of thermal waves in a turbulent fluid—cryogenic helium gas. They differ in many important ways from the thermal waves in turbulent superfluids displaying the two-fluid phenomena; one striking difference is that whereas the attenuation of the former decreases with the turbulence intensity (Ra), the presence of quantized vortices increases the attenuation of the latter, known as second sound in turbulent superfluids. We have developed two physically motivated models capturing the observed properties of thermal waves: in particular, constructive and destructive interference of two coherent thermal waves generated by harmonically modulating the temperatures of the top and bottom plates of the RBC cell. The more complex phenomena occurring in BLs under temperature modulation, such as enhancement of heat transfer efficiency, are not described, as the key quantity of Model 1, the spatially dependent effective thermal diffusivity κ_{eff} is based on the undisturbed steady-state temperature profile of the RBC flow. Interference of thermal waves, mediated in turbulent fluids by κ_{eff} much higher than the molecular thermal diffusivity brings new information, reminiscent of the effective kinematic viscosity in the ocean or atmospheres of the Earth or planets, which has a tremendous impact for example on the behavior of internal gravity waves and, therefore, the energy budget. We hope that our results will stimulate further interest in thermal waves and their utilization in order to study various aspects of turbulent flows and their BLs.

ACKNOWLEDGMENTS

APPENDIX

1. Model 1: Thermal waves propagating in turbulent RBC flow and their interference

The model solves the one-dimensional parabolic heat diffusion equation taking into account the known steady-state temperature profile $T_0(z)$ of the turbulent RBC flow with the coordinates chosen so that the z axis points along the vertical axis of the RBC cell of height L. In particular, we use the analytical expression for the dimensionless temperature profile of the thermal BL obtained for $\mathrm{Pr} \approx 1$ by Shishkina *et al.* [27],

$$\theta = \frac{\sqrt{3}}{4\pi} \ln \frac{(1 + a\xi)^3}{1 + (a\xi)^3} + \frac{3}{2\pi} \arctan\left(\frac{4\pi}{9}\xi - \frac{1}{\sqrt{3}}\right) + \frac{1}{4}, \tag{A1}$$

where $a = 2\pi/3\sqrt{3} \approx 1.2$ and a local similarity variable $\xi = z/\delta(x)$ where $\delta(x)$ stands for the local BL thickness, which we approximate as $\delta(x) \approx \delta = L/(2\,\mathrm{Nu})$. As the profiles of two BLs need to be joined together smoothly at the half-height of the cell, a suitable linear background is added that guarantees continuous temperature values and their derivatives at $z = L/2$ with negligible overall effect on the simulation results.

The inhomogeneous heat equation is given as

$$\frac{\partial T(z,t)}{\partial t} = \frac{\partial}{\partial z}\left[\kappa_{\mathrm{eff}}(z)\frac{\partial T(z,t)}{\partial z}\right], \tag{A2}$$

where $\kappa_{\mathrm{eff}}(z)$ is a spatially dependent effective thermal diffusivity, independent of temperature. The heat flux $\dot{q}(z,t)$ is given by the term inside the bracket.

Assuming a harmonic variation of temperature, solution is sought in the general form $T(z,t) = T_0(z) + T_1(z)\exp(i\omega_1 t) + T_2(z)\exp(i\omega_2 t)$, where ω_1 and ω_2 are the frequencies of temperature modulations of the top and bottom plates, respectively, with T_1 and T_2 the respective complex amplitudes. For the case $\omega_1 = \omega_2$, naturally only one oscillating term would be used.

After substitution into Eq. (A2) and separating the time-dependent terms, we get

$$0 = \frac{d}{dz}\left(\kappa_{\mathrm{eff}}(z)\frac{dT_0(z)}{dz}\right), \tag{A3}$$

$$i\omega_n T_n(z) = \frac{d}{dz}\left(\kappa_{\mathrm{eff}}(z)\frac{dT_n(z)}{dz}\right), \tag{A4}$$

immediately allowing us to define $\kappa_{\mathrm{eff}}(z)\frac{dT_0(z)}{dz} \equiv c$ from Eq. (A3), to satisfy the steady-state condition. The constant c is chosen so that $\kappa_{\mathrm{eff}}(z=0) \equiv \kappa$. Equation (A4) is then solved for one or two different frequencies used (as the case might be) subject to the experimental boundary conditions, typically prescribing the complex modulation amplitudes T_n at both plates. We note that this model tends to underestimate the temperature wave amplitudes in the bulk. This is caused by the fact that κ_{eff} is determined from the steady-state boundary layer only, i.e., no modulation of the boundary layer properties is taken into account. A full-fledged description of the complex phenomena occurring in boundary layers under temperature modulation, such as effects related to the ejection of thermal plumes, is beyond the scope of this simple one-dimensional model. Additional inaccuracy stems from the fact that the BL profile in Eq. (A1) from Ref. [27] is derived under the assumption that Pr slightly exceeds unity, explicitly using the fact that the velocity BL thickness exceeds the thermal one (a linear tangential velocity profile is assumed in the entire thermal boundary layer). However, our experiments are performed at Pr = 0.74, i.e., the thermal BL is thicker, and a part of it may be effectively bypassed owing to turbulent velocity fluctuations. Formally, the model may be adjusted to match the experimental observations perfectly by using a higher value of the a parameter, but this would lack physical justification as the model would become internally inconsistent. We have attempted to improve the model under the assumption of fully matched BLs (Pr = 1), but the improvement yielded was rather small and insufficient to account for the difference between experiment and theory. This leaves the modulation of the boundary layer properties as the most likely cause for this mismatch, and we believe that any full-fledged description will have to account for it explicitly.

The numerical solution is written in PYTHON and uses the procedure SOLVE BVP from the SCIPY package. To improve numerical convergence of the boundary problem solver, it is advantageous to rescale the discretized z coordinates with steps inversely proportional to $\kappa_{\mathrm{eff}}(z)$.

An example of the steady temperature profile and the z dependence of effective thermal diffusivity for Nu = 232.7 is illustrated in Fig. 4.
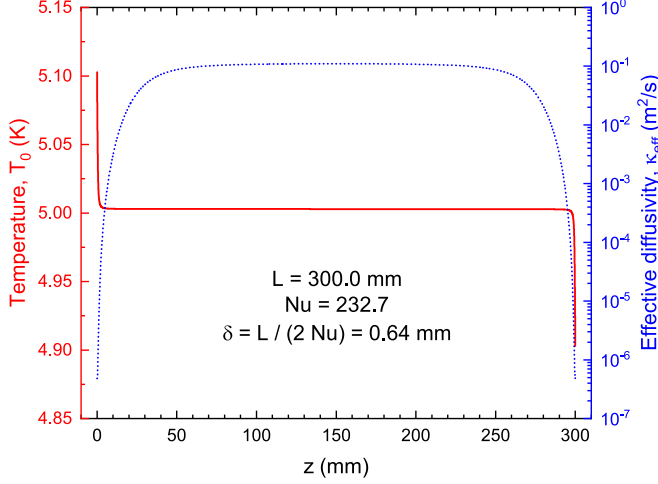
FIG. 4. Illustrative example of the steady temperature profile (red, left axis) and the effective thermal diffusivity (blue, right axis) within the model. The linear background discussed in the text is imperceptible in the temperature profile but imposes an upper limit on the effective diffusivity $\kappa_{\mathrm{eff}}(z)$ in the center of the cell, usually, at least, five orders of magnitude above κ, approximating the superconducting core suggested by Niemela and Sreenivasan [22].

Model 2: Simple analytical model of modulated RBC possessing a superconducting core

The model considers a high-Ra RBC heat flow in a (cylindrical) cell of height L. Both top and bottom plates as well as the bulk of the turbulent RBC flow are assumed to be ideal heat conductors; the superconducting [22] bulk core being surrounded by thin thermal boundary layers adjacent to the top and bottom plates, of thermal conductances Λ_t and Λ_b, thicknesses $\delta = L/(2\,\mathrm{Nu}) \ll L$, both of negligibly small thermal capacity. For the sake of simplicity, the bottom plate temperature $T_b = T_{b0} = const$, whereas the top plate temperature is harmonically modulated: $T_t = T_{t0} + A_t e^{i\omega t}$, where $\omega = 2\pi f_m$. We avoid heat transfer enhancement assuming that $A_t \ll \Delta = T_{b0} - T_{t0}$ [11,21]. We seek the solution for the temperature of the bulk core in the form $T_c(t) = T_{c0} + A_c e^{i(\omega t - \phi)}$.

The thermal balance of the turbulent core reads

$$C_c dT_c(t) = (\dot{Q}_b - \dot{Q}_t)dt, \tag{A5}$$

where C_c is the heat capacity of the bulk core and $\dot{Q}_b$ ($\dot{Q}_t$) denotes the heat flux from the bottom (to the top) plate,

$$\dot{Q}_b = \Lambda_b[T_{b0} - T_{c0} - A_c e^{i(\omega t - \phi)}], \tag{A6}$$

$$\dot{Q}_t = \Lambda_t[T_{c0} - T_{t0} + (A_c e^{-i\phi} - A_t)e^{i\omega t}]. \tag{A7}$$

By substituting to Eq. (A5) and separating its constant and time-dependent parts, we obtain

$$(i\omega C_c + \Lambda_b + \Lambda_t)A_c e^{i(\omega t - \phi)} - \Lambda_t A_t e^{i\omega t} = \Lambda_b[T_{b0} - T_{c0}] - \Lambda_t[T_{c0} - T_{t0}]. \tag{A8}$$

To be valid at all times, both sides of Eq. (A8) must be equal to zero.

From the right-hand side, we get the equilibrium value of T_c,

$$T_{c0} = \frac{\Lambda_b T_{b0} + \Lambda_t T_{t0}}{\Lambda_b + \Lambda_t}. \tag{A9}$$

Assuming equal conductivities of the top and bottom boundary layers $\Lambda_b = \Lambda_t$, we arrive at the usual result $T_{c0} = (T_{b0} + T_{t0})/2$.

The left-hand side, after removing the time dependence, reads

$$(i\omega C_c + \Lambda_b + \Lambda_t)A_c e^{-i\phi} - \Lambda_t A_t = 0. \tag{A10}$$

Equating both the real and the imaginary terms separately to zero allows to determine the unknown phase ϕ and temperature modulation A_c of the bulk,

$$\tan \phi = \frac{\omega C_c}{\Lambda_b + \Lambda_t} \approx \frac{\omega C_c}{2\Lambda}, \tag{A11}$$

$$A_c = A_t \frac{\Lambda_t}{\Lambda_b + \Lambda_t} \cos \phi \approx \frac{A_t}{2} \cos \phi. \tag{A12}$$

We see that, for $\omega \to 0$, the phase-shift $\phi \to 0$ for small ω, it increases approximately linearly and in the high-frequency limit the phase shift saturates at $\pi/2$ whereas $A_c \to 0$.

It is easy to extend the model for the case when temperatures of both top and bottom plates are harmonically modulated, for simplicity, with the same amplitude $A_b = A_t = A$ and frequency f_m. For the two cases—(i) modulation in phase: we have $A_c = A_t$ (constructive interference) and (ii) out of phase $A_c = 0$ (destructive interference).

---

[1] J. A. Scales, and R. Snieder, What is a wave? Nature (London) **401**, 739 (1999).

[2] D. D. Joseph, and L. Preziosi, Heat waves, Rev. Mod. Phys. **61**, 41 (1989).

[3] A. J. Angström, New method of determining the thermal conductibility of bodies, London, and Edinburgh Dublin Philos. Mag. J. Sci. **25**, 130 (1863).

[4] C. Cattaneo, Sulla conduzione de calore, *Atti del Semin. Mat. e Fis. Univ. Modena 3*, 3 (1948).

[5] C. Cattaneo, A form of heat conduction equation which eliminates the paradox of instantaneous propagation, Comptes Rendus **247**, 431 (1958).

[6] E. Varga, M. D. Jackson, D. Schmoranzer, and L. Skrbek, The use of second sound in investigations of quantum turbulence in He II, J. Low Temp. Phys. **197**, 130 (2019).

[7] S. Midlik, D. Schmoranzer, and L. Skrbek, Transition to quantum turbulence in oscillatory thermal counterflow of 4He, Phys. Rev. B **103**, 134516 (2021).

[8] A. Beardo, M. López-Suárez, L. A. Pérez, L. Sendra, M. I. Alonso, C. Melis, J. Bafaluy, J. Camacho, L. Colombo, R. Rurali, F. X. Alvarez, and J. S. Reparaz, Observation of second sound in a rapidly varying temperature field in Ge, Sci. Adv. **7**, eabg4677 (2021).

[9] G. Ahlers, S. Grossmann, and D. Lohse, Heat transfer and large-scale dynamics in turbulent Rayleigh-Bénard convection, Rev. Mod. Phys. **81**, 503 (2009).

[10] F. Chilla, and J. Schumacher, New perspectives in turbulent Rayleigh-Bénard convection, Eur. Phys. J. E **35**, 58 (2012).

[11] P. Urban, P. Hanzelka, T. Králík, V. Musilová, and L. Skrbek, Thermal Waves and Heat Transfer Efficiency Enhancement in Harmonically Modulated Turbulent Thermal Convection, Phys. Rev. Lett. **128**, 134502 (2022).

[12] G. Venezian, Effect of modulation on the onset of thermal convection, J. Fluid Mech. **35**, 243 (1969).

[13] J. J. Niemela, and R. J. Donnelly, External Modulation of Rayleigh-Bénard Convection, Phys. Rev. Lett. **59**, 2431 (1987).

[14] Q. W. Wang, G. Wang, M. Zeng, and H. Ozoe, Uni-directional heat flux through the horizontal fluid layer with sinusoidal wall temperature at the top or bottom boundaries, Int. J. Heat Mass Transf. **51**, 1675 (2008); Upward heat flux through the horizontal fluid layer of water with sinusoidal wall temperature at the top or bottom boundary, Numer. Heat Transfer, Part A **52**, 817 (2007).

[15] A. Raji, M. Hasnaoui, M. Firdaouss, and C. Ouardi, Natural convection heat transfer enhancement in a square cavity periodically cooled from above, Numer. Heat Transfer, Part A **63**, 511 (2013).

[16] P. Urban, P. Hanzelka, T. Králík, V. Musilová, L. Skrbek, and A. Srnka, Helium cryostat for experimental study of natural turbulent convection, Rev. Sci. Instrum. **81**, 085103 (2010).

[17] According to the Calibration Certificate issued by PTB Berlin, the expanded uncertainty of the calibration of our GR-200A-1500 sensor is 2 mK in the range of 1.78 to 10.45 K.

[18] microsensor.com.ua.

[19] V. F. Mitin, P. C. McDonald, F. Pavese, N. S. Boltovets, V. V. Kholevchuk, I. Yu. Nemish, V. V. Basanets, V. K. Dugaev, P. V. Sorokin, R. V. Konakova, E. F. Venger and E. V. Mitin, Ge-on-GaAs film resistance thermometers for cryogenic applications, Cryogenics **47**, 474 (2007).

[20] V. F. Mitin, V. V. Kholevchuk and B. P. Kolodych, Ge-on-GaAs film resistance thermometers: Low-temperature conduction and magnetoresistance, Cryogenics **51**, 68 (2011).

[21] R. Yang, K. L. Chong, Q. Wang, R. Verzicco, O. Shishkina, and D. Lohse, Periodically Modulated Thermal Convection, Phys. Rev. Lett. **125**, 154502 (2020).

[22] J. J. Niemela, and K. R. Sreenivasan, Formation of the "Superconducting" Core in Turbulent Thermal Convection, Phys. Rev. Lett. **100**, 184502 (2008).

[23] J. Ordonez-Miranda, R. Anufriev, M. Nomura, and S. Volz, Net heat current at zero mean temperature gradient, Phys. Rev. B **106**, L100102 (2022).

[24] R. D. McCarty, National Bureau of Standards Technical Note No. 631 (1972); V. D. Arp and R. D. McCarty, The properties of critical helium gas, Technical Report, University of Oregon (1998).

[25] C. H. B. Priestley, *Turbulent Transfer in the Lower Atmosphere* (University of Chicago Press, Chicago, 1959).

[26] W. V. R. Malkus, Heat transport and spectrum of thermal turbulence, Proc. R. Soc. London, Ser. A **225**, 196 (1954).

[27] O. Shishkina, S. Horn, S. Wagner, and E. S. C. Ching, Thermal Boundary Layer Equation for Turbulent Rayleigh–Bénard Convection, Phys. Rev. Lett. **114**, 114302 (2015).

[28] D. Lohse, and F. Toschi, Ultimate State of Thermal Convection, Phys. Rev. Lett. **90**, 034502 (2003).

[29] P. Urban, P. Hanzelka, T. Králík, V. Musilová, A. Srnka, and L. Skrbek, Effect of Boundary Layers Asymmetry on Heat Transfer Efficiency in Turbulent Rayleigh-Bénard Convection at Very High Rayleigh Numbers, Phys. Rev. Lett. **109**, 154301 (2012).

[30] P. Urban, P. Hanzelka, V. Musilová, T. Králík, M. La Mantia, A. Srnka, and L. Skrbek, Heat transfer in cryogenic helium gas by turbulent Rayleigh-Bénard convection in a cylindrical cell of aspect ratio 1, New J. Phys. **16**, 053042 (2014).

[31] P. Urban, T. Králík, M. Macek, P. Hanzelka, T. Věžník, and L. Skrbek, Effect of boundary conditions in turbulent thermal convection, Europhys. Lett. **134**, 34003 (2021).